SUPPLEMENTARY MATERIAL

The Real McCoy: Great Unconformity source to sink on the rifted passive margin of western Laurentia

Eliel Anttila[1], Francis A. Macdonald[1], Joneel Zinto[2], and Max D. Britt[3]
[1]*Department of Earth Science, University of California, Santa Barbara, CA 93106, USA*
[2]*Department of Geology, University of Kansas, Lawrence, KS 66045, USA*
[3]*Department of Geosciences, University of Arizona, Tuscon, AZ 85721, USA*

SUMMARY

This document includes detailed methods for all geochronological and geochemical analyses, a summary of parameters and inputs for the tectonic subsidence model, a summary of U-Pb zircon geochronology analytical results, a summary of carbonate stable carbon isotopic analytical results, four supplementary figures, formalization tables for two new formations in the McCoy Creek Group (Table SM1), geochronological data (Table SM2), chemostratigraphic data (Table SM3), and a tabulated summary of tectonic subsidence model inputs (Table SM4).

1:24,000 geologic maps of the central Schell Creek Range and northern Egan Range study areas are included as Supplementary Maps 1 and 2, respectively.

All supplementary material, data, and code for this work is accessible within the following GitHub repository: https://github.com/eliel-anttila/Anttila_et_al_McCoy_2024

METHODS

Between 2020-2023, we mapped exposures of the McCoy Creek Gp in the Schell Creek and Egan Ranges of Nevada and the Deep Creek Range of Utah with iPads running FieldMove digital mapping software. Stratigraphic sections were measured using meter-sticks. Samples for carbon isotope chemostratigraphy and U-Pb zircon geochronology were collected within measured stratigraphic sections, or from localities in which the relative stratigraphic height of the sample was easily calculated from map relationships.

Zircon Geochronology

Sample collection

Samples collected for detrital zircon geochronology are described below, in ascending stratigraphic order:

F2005-273.4/275*—Trout Creek Group Unit 3:* The sandstone matrix of diamictite with clasts of amphibolite (Fig. 3C) was collected along the north side of Trout Creek in the Deep Creek Range at 39.7466°N, 113.8884°W. Two horizons directly above amphibolite horizons ~120 m above the base of Unit 3 were sampled.

TC4-1*—Trout Creek Sequence Unit 4:* A poorly sorted arkosic wacke, featuring subangular plagioclase rhombs, was sampled from Trout Creek Sequence Unit 4 on a ridge north of Trout Creek in the Deep Creek Range at 39.7506ºN, 113.8924ºW. The sampled horizon is located just below a fine arenitic sandstone horizon containing isolated dropstones (Fig. 2d).

F2003-3*—Trout Creek Group Unit 7:* A white, vitreous quartzite with 0.5-meter-scale tabular cross bedding was sampled one meter below the base of the upper diamictite of Trout Creek Unit 7 on the north side of McCoy Creek in the Schell Creek Range at 39.3747°N, 114.5289°W.

F2002-204.9*—Yelland formation:* Fine-grained sandstone from a 10-cm-thick graded bed was sampled 91.4 meters above the base of the Yelland Formation on the south side of McCoy Creek in the Schell Creek Range at 39.3723°N, 114.5301°W.

F2002-273.4—*Bassett Formation:* A ~10 cm thick bed of medium-grained arenitic sandstone ~50 m above the base of the Bassett Formation was sampled on the south side of McCoy Creek at 39.3718ºN, 114.5318ºW.

MC_2—*Bassett Formation:* A medium-coarse arenite at the lowest exposure of the Debrah Mb of the Bassett Fm was sampled on the ridge north of McCoy Creek at 39.3778ºN, 114.5361ºW.
Egan 182.0*—Egan Formation:* A medium-to-coarse subarkosic litharenite bed, ~20cm thick and interbedded within brown-green argillite, was sampled from the slope above the north side of Egan Creek in the Egan Range at 39.8662°N, 114.9228°W.

Egan 233.0*—Egan Formation:* Coarse grained arkosic grit with basal shale rip-ups and occasional laterally discontinuous grit channels was sampled from the middle Egan Fm along the north side of Egan Creek in the Egan Range at 39.8651ºN, 114.9240°W.

Egan 384.4*—Willard Creek Quartzite:* Half meter- to meter-thick beds of coarse arenitic quartzite with minor amalgamated granule-cobble conglomerate was sampled from the Willard Fm at Egan Creek at 39.8659ºN, 114.9256°W.

Egan 564.0*—Strawberry Creek Formation:* Poorly sorted subarkosic pebble conglomerate with interbeds of coarse litharenitic sandstone was sampled from the middle Strawberry Creek Fm at Egan Creek at 39.8652ºN, 114.9281°W.

Sample preparation

Geochronology samples were trimmed with a rock saw and cleaned to remove potential surficial contamination, and pulverized in an industrial jaw crusher. The resultant <500 micron grainsize fraction was collected, and subsequently washed in an antiflocculant solution to remove ultrafine material. Samples were then panned to isolate heavy minerals. Samples containing few zircon crystals were further magnetically separated with a Frantz device (0.4A at a 20º incline), and put through a final density separation in methylene iodide. Zircon grains were individually picked from resultant heavy mineral separates, annealed in a muffle furnace for 48 hours at 900ºC, mounted in epoxy, and polished. The internal structures of the grains were mapped with cathodoluminescence (CL) imaging using a Cameca SX-100 Electron Probe Micro-Analyzer (EPMA) with a CL detector.

Laser ablation inductively coupled plasma mass spectrometry (LA-ICPMS) analyses

LA-ICP-MS U-Pb geochronological analyses on zircon were completed at UCSB, using a Cetac/Photon Machines Analyte Excite 193 nm excimer laser attached to a Nu Plasma 3D multicollector ICPMS, following the methods of Kylander-Clark et al. (2013). Each zircon was ablated with a 20µm laser spot. The zircon 91500 (Wiedenbeck et al., 1995) was used for age calibration. Secondary zircon reference materials included 9435, AUSZ, Mudtank, GJ1, and Plesovice (Jackson et al., 2004). *Iolite* (Paton et al., 2010) was used to correct for U-Pb mass bias and drift following the methods of Kylander-Clark et al. (2013) and Horstwood et al. (2016). The resultant U and Pb isotopic ratios were reduced according to methods outlined in Kylander-Clark et al., 2013. Dates for each analyzed grain were calculated by importing reduced $^{238}U/^{206}Pb$ and $^{207}Pb/^{206}Pb$ ratios into *IsoplotR (Vermeesch, 2018).* All LA-ICP-MS data is collated in Table SM2. We also retabulate data from Yonkee et al., 2014, which were integrated into the normalized probability plots described below.

Normalized probability plots

Detrital zircon normalized probability plots were created for all detrital samples. Discordant analyses from detrital samples were removed by excluding all ages exhibiting more than 15% discordance. Concordia ages (Vermeesch, 2020) from the resultant filtered dataset from each sample were combined with other samples from the same formation (including extant data from Yonkee et al., 2014), and were incorporated into a kernel density estimation (KDE) function (full code available in GitHub repository) to generate the normalized probability plots depicted in Fig. 9 of the main manuscript. Maximum depositional ages from detrital samples were calculated by isolating groups of young zircon analyses conforming to the MSWD (Wendt and Carl, 1991) criteria for a single magmatic population of *n* grains (Spencer et al., 2016).

Carbonate Geochemistry

Carbonate samples were collected from within measured stratigraphic sections, and were subsequently slabbed and microdrilled to procure aliquots of carbonate powder at the University of California, Santa Barbara. Carbonate $\delta^{13}C$ and $\delta^{18}O$ data were acquired at the Center for Stable Isotope Biogeochemistry at the University of California, Berkeley. Between 10-100 microgram subsamples of each powder aliquot were reacted with concentrated H_3PO_4 at 90°C for 10 mins to generate CO_2 gas for coupled $\delta^{13}C$ and $\delta^{18}O$ analysis using a GV IsoPrime mass spectrometer with Dual-Inlet and MultiCarb systems. Several replicates of one international standard NBS19, and two lab standards $CaCO_3$-I & II were measured along with approximately 40 unknowns for each run. The overall external analytical precision was about $\pm$0.05‰ for $\delta^{13}C$ and about $\pm$0.07‰ for $\delta^{18}O$. All carbonate chemostratigraphic data and section locations are collated in Table SM3.

Tectonic subsidence model

Representative stratigraphic thicknesses, lithological information, and inferred depositional environments were utilized to develop a tectonic subsidence curve for the entirety of the Trout Creek Sequence and McCoy Creek Group, as well as the overlying Paleozoic succession (through the Ely Limestone) within the model framework of Zhang et al. (2023a,b). All inputs for this portion of the model can be viewed in the first sheet ("Stratigraphy") of Table SM4; a detailed discussion of the SubsidenceChron.jl model framework (and parameters therein) can be viewed within Zhang et al. (2023a,b).

Stratigraphic age constraints were integrated into a Bayesian age-height model framework (Schoene et al., 2019), encapsulated within the model framework of Zhang et al. 2023b), to generate model ages for all stratigraphic heights included within the tectonic subsidence curve model. Age controls for the Trout Creek Sequence and McCoy Creek Group, based on the age framework depicted in Fig. 6, are collated in the second sheet ("Age_control") of Table SM4. An estimated maximum depositional age of strata below Trout Creek Sequence Unit 1, with large approximated uncertainty, was included to allow a continuous age-height curve to be modeled through the base of Unit 1. Paleozoic age controls include the base of the Pioche Shale, which can be correlated with the ca. 507 Ma base of the Bright Angel Shale (Karlstrom et al., 2020), the ca. 493 Ma SPICE positive carbon isotope excursion (Cothren et al., 2022) which is hosted by the Dunderberg Shale, a ca. 469 Ma biostratigraphic age constraint from the top of the Pogonip Group (Edwards and Saltzman, 2014; Gradstein et al., 2020) and a minimum depositional age at the top of the Lower Pennsylvanian Ely Limestone (Long et al., 2022). The age-height model was then used to generate interpolated ages for all stratigraphic heights integrated into the tectonic subsidence curve, allowing tectonic subsidence to be plotted against time (blue curve, Fig. 8a).

The age-height model was also used to generate a model undecompacted sedimentation rate curve. Note that we include an age control point at the base of Marinoan glacial strata (diamictite sequence of Trout Creek Sequence Unit 7), with an estimated glacial onset age of ~640 Ma, in line with the conservative estimate used to calculate the linear Cryogenian sedimentation rates depicted with the dashed purple line in Fig. 8a. The incorporation of this approximate constraint does not appreciably change the structure of the tectonic subsidence curve, but allows for a better representation of sedimentation rate changes across the Cryogenian in the sedimentation rate model. All code used to generate the tectonic subsidence model and sedimentation rate curve depicted in Fig. 8a can be viewed within the following GitHub repository:(/Anttila_et_al_McCoy_2024/Bayesian_Subsidence/McCoy_Subsidence_Bayesian.ipynb).

A McKenzie-style idealized thermal subsidence curve was fit to the tectonic subsidence curve by generating posterior distributions of the timing of thermal subsidence onset (T_0) and the crustal stretching factor (β) (Fig. 8c), which were then repeatedly sampled to generate a range of possible thermal subsidence curves (red curve, Fig. 8b). All calculated thermal subsidence curves utilize a lithospheric cooling constant, τ, of 60 Ma. The initial choice of a prior T_0 was informed by geological evidence from the Cordilleran Laurentian margin, which suggests the occurrence of active rifting in the Cryogenian as evidenced by syn-extensional Cryogenian deposition in Death Valley (Macdonald et al., 2013; Nelson et al., 2020) and Cryogenian volcanism in Idaho (Isakson et al., 2022, Keeley et al., 2013). With a mid-Cryogenian (T_0=651±5 Ma,1s) rift-drift transition prior set, beta-factor priors were then iteratively increased until β=5.5±.75 (1s), which resulted in the modeled tectonic subsidence curve being well-matched by idealized thermal subsidence curves generated from the resultant posterior β and T_0 distributions (Fig. 8b,c). All code (modified from Zhang et al., 2023b) used to generate the tectonic subsidence curve and thermal subsidence curves and posterior parameter distributions in Fig. 8b,c can be viewed within following directory of the GitHub repository: (/Anttila_et_al_McCoy_2024/Bayesian_Subsidence/McCoy_SHORT_Subsidence_Bayesian.ipynb).

ANALYTICAL RESULTS

U-Pb Zircon Geochronology

Sandstone samples were collected through the Trout Creek Gp and McCoy Creek Gp in the Deep Creek, Schell Creek, and Egan Ranges to compliment the previous detrital zircon geochronological dataset of Yonkee et al. (2014) from the Deep Creek Range. Sample locations and new LA-ICPMS zircon data are collated in Table SM2. From TCU3, sample F2005-273.4/275 yielded an age spectrum with dominantly Stenian peaks, while sample TC4-1, from TCU4, features a spectrum with Stenian peaks, as well as a young peak that can be discretized into two distinct magmatic populations (688.5±2.44 Ma, n=6; 696.9±3.40 Ma, n=3; Fig. 1). From TCU7, sample F2003-3 yielded a dominant Stenian peak in the detrital zircon spectrum, with subsidiary 1300-1500Ma peaks. Sample F2002-204.9 from the Yelland Fm yielded a dominant peak around 1300 Ma, while samples F2002-273.4 and MC_2 combined to yield dominant Stenian and 1300-1500Ma (syn-Picuris) peaks in the Bassett fm. The Egan Fm, represented by samples Egan 182.0 and Egan 233.0, features a dominant stenian peak and subsidiary syn-Picuris peak, while sample Egan 384.4 from the Willard Creek Quartzite and sample Egan 564.0 from the Strawberry Creek Fm display a similar pattern in the composite detrital zircon age spectrum for each respective unit. Sample M1901-10.25 from the Osceola Argillite yields a detrital zircon spectra with a dominant age peak between 1600-1800Ma, with a conspicuous lack of Stenian zircon. All detrital spectra, including those incorporating data from this study and those of Yonkee et al., 2014, are shown in Fig. 9 in the main manuscript.

Carbonate carbon and oxygen isotope analyses

We report 164 carbonate carbon ($\delta^{13}C$) and oxygen ($\delta^{18}O$) isotope analyses from the Trout Creek Sequence and the McCoy Creek Gp; all carbonate carbon and oxygen isotopic data, and sampling locations, are collated in Table SM3. $\delta^{13}C$ values from Unit 2 of the Trout Creek Sequence vary from 0 to +4 ‰, and average +1.8 ‰. $\delta^{18}O$ values vary from -5 to -16 ‰, average -9.3 ‰, and do not show significant covariance with $\delta^{13}C$. Three measurements from carbonates in the ~20 cm thick cap carbonate have $\delta^{13}C$ values between -4.2 and -6.4 ‰, and $\delta^{18}O$ values that average -16.5 ‰. Two carbonate intervals within the upper portions Unit 7 of the Trout Creek Sequence were sampled for carbonate chemostratigraphy, and host $\delta^{13}C$ values between +5 and +9‰, with most values clustering between +7 and +8‰. The 8 m-thick cap dolostone of the basal Yelland Fm of the McCoy Creek Gp was sampled at 0.5 m resolution. These 16 samples have consistent $\delta^{13}C$ values between -2.3 and -2.9 ‰, and $\delta^{18}O$ values between -9.4 and -11.2 ‰ (Table SM3). Higher in unit B, $\delta^{13}C$ values in limestones become more variable, but remain negative and do not covary with $\delta^{18}O$.

The Osceola Fm of the McCoy Creek Gp was sampled for carbonate chemostratigraphy in the S. Snake Range and the Pilot Range. In the S. Snake Range, four samples were analyzed from the ~20 cm thick limestone horizon. The lower horizon yielded $\delta^{13}C$ values of -11.37 and -11.24 ‰, and the upper horizon yielded $\delta^{13}C$ values of -9.19 and -9.39. In the Pilot Range, $\delta^{13}C$ values increase up-section from ~-9.5 to -8.5 ‰ over a 70m interval.

Fig. SM1

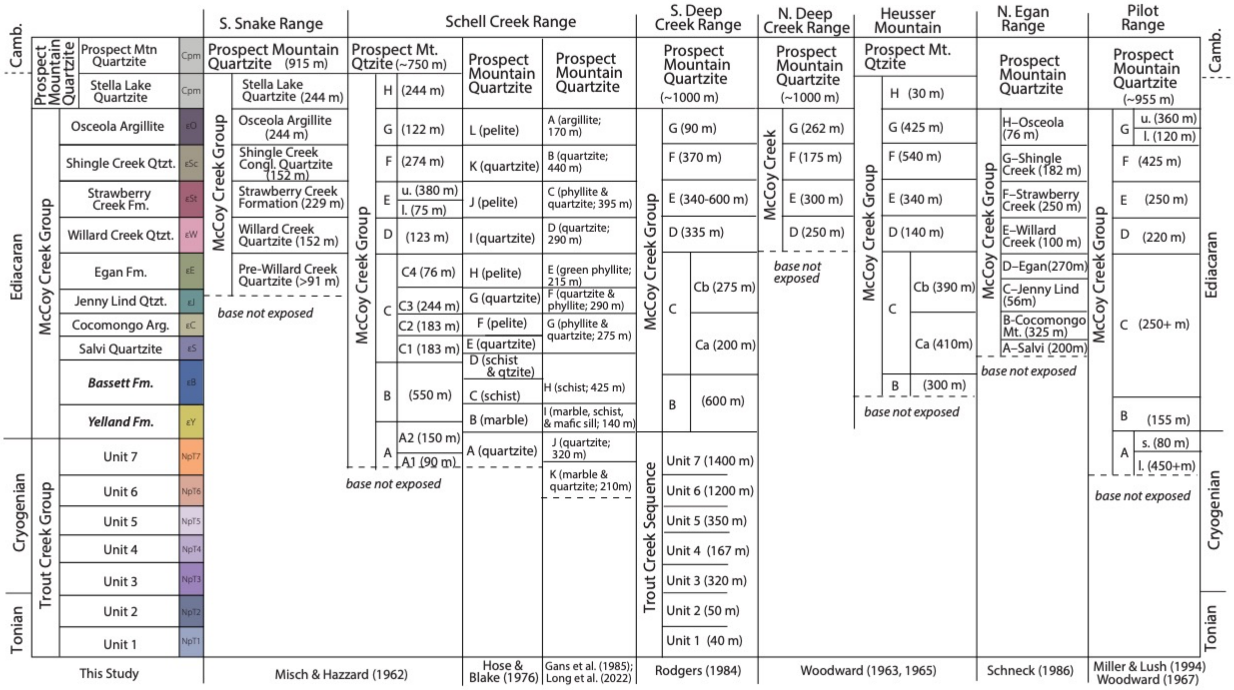

Figure SM1: Unit nomenclature for the Trout Creek Sequence and McCoy Creek Group, including previous naming schemes (right) and the full stratigraphic nomenclature (including map unit colors and symbols) used in this study (left). Note that the new nomenclature is an amalgamation of the naming schemes of Misch and Hazzard (1962), Rodgers (1984), and Schneck (1986); two new formalized units are highlighted with bold italicized text. Formalization tables for the Yelland Fm and Bassett Fm can be found in Table SM1.

Fig. SM2

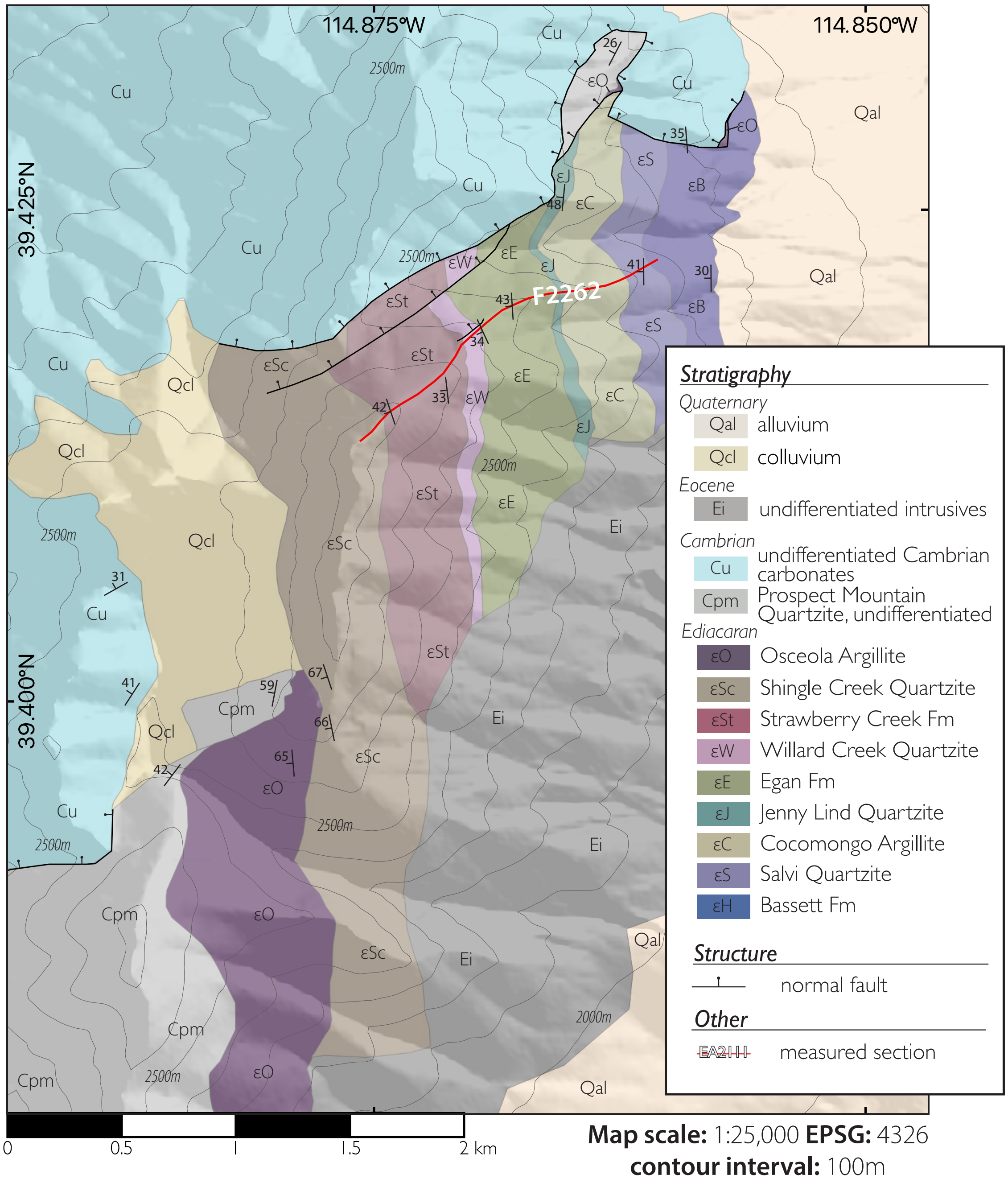

Figure SM2: Geologic map of the Heusser Mountain study area (see Fig. 1b). In addition to measured section F2262, a schematic section through the Osceola Fm (Fig. 5 inset) at this locality was approximated from map relationships and geometries.

Fig. SM3

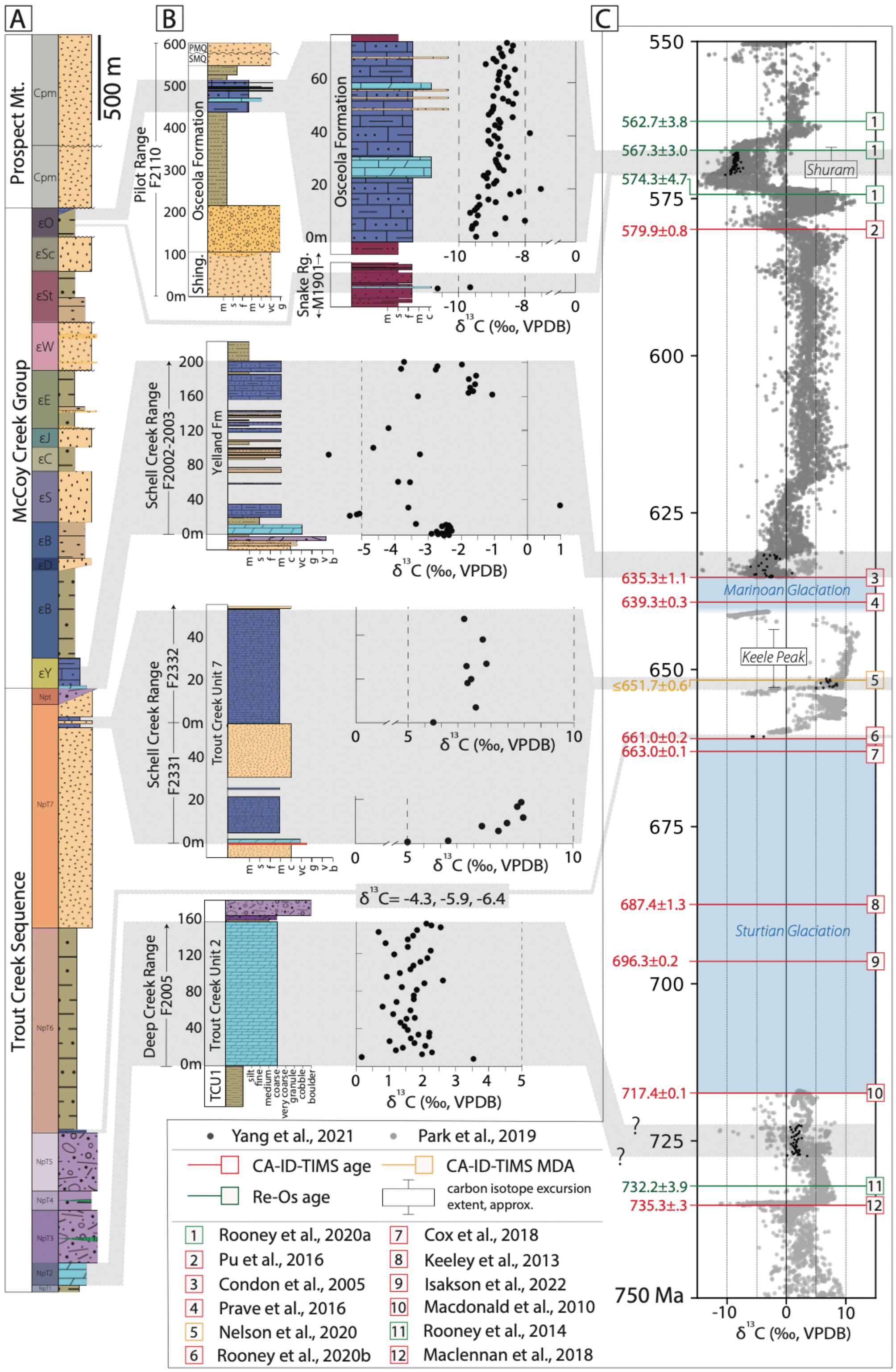

Figure SM3: Version of Figure 6 from main manuscript, with references for all geochronological constraints. A) Generalized lithostratigraphy of the Trout Creek Sequence and McCoy Creek Group. **B)** Carbonate δ^{13}C chemostratigraphy of the Trout Creek Sequence and McCoy Creek Group, correlated with **C)** a compiled global Tonian-Ediacaran δ^{13}C chemostratigraphy, amalgamated from the compilations of Yang et al. (2021) and Park et al. (2019). All chemostratigraphic data from this study, including sampling location coordinates, are compiled in Table SM3.

Fig. SM4

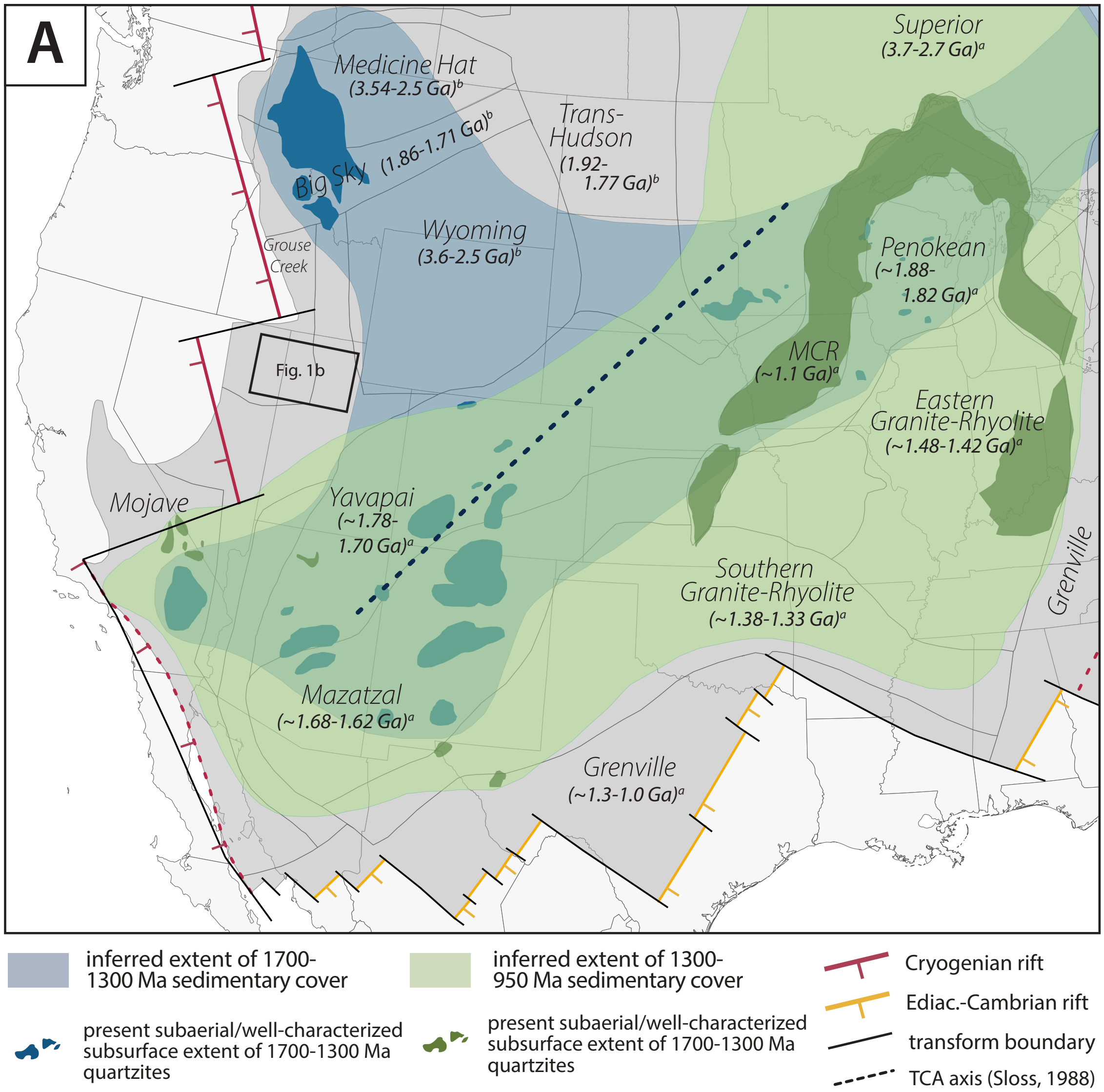

Figure SM4. Version of Figure 10A, including references to graphical components of the figure. Proterozoic sedimentary cover of Laurentia, schematically depicting the inferred extent of pre-Grenville sedimentary cover (transparent blue polygon) and overlying Stenian (syn-Grenville) sediments (transparent green polygon). Remnant pre-Grenville quartzites, including modern outcrop and well-characterized subsurface extents, are depicted in dark blue (modified from Carlson, 1970; Southwick et al., 1986; Jones III and Thrane, 2012, Medaris et al., 2021, Mahatma et al., 2022, and Brennan et al., 2021). We infer the extent of pre-Stenian sedimentary cover by broadly outlining the extent of these remnant outcrops and subsurface occurrences. The surface outcrop and well-characterized subsurface extent of Stenian syn-Grenville quartzites, including the Middle Run Fm (Clay et al., 2021) in the subsurface of Indiana Ohio, and Kentucky, the Jacobsville Fm (Hodgin et al., 2022) of the Midcontinent, the Hazel and Lanoria Formations (Spencer et al., 2014) of Texas, the Unkar Group (Timmons et al., 2012) of Arizona, the Crystal Springs Formation (Mahon et al., 2014) of California, and distal basins in the Canadian Arctic (Rainbird et al., 2012) are depicted with dark green polygons. We infer the putative extent of syn-Grenville sedimentary cover by outlining the extent of Stenian quartzite outcrops and subsurface occurrences, and extend this polygon to cover a consistent distance inboard of the Grenville front; this distance is a conservative estimate for pro-Grenville sediment extent, given evidence for long-traveled pro-Grenville sedimentation in northwest Canada (Rainbird et al., 2012). The extent of the Laurentian craton (dark gray) and rift positions/extents are modified from Macdonald et al., 2022 and Poole et al., 2005; ages and extents of cratonic basement provinces (italicized labels) are compiled from Clay et al., 2021(a) and Brennan et al., 2021(b).

REFERENCES

Brennan, D. T., Mahoney, J. B., Li, Z. X., Link, P. K., Evans, N. J., & Johnson, T. E. (2021). Detrital zircon U–Pb and Hf signatures of Paleo-Mesoproterozoic strata in the Priest River region, northwestern USA: A record of Laurentia assembly and Nuna tenure. *Precambrian Research*, *367*, 106445. https://doi.org/10.1016/j.precamres.2021.106445

Carlson, M. P. (1970). Distribution and subdivision of Precambrian and Lower and Middle Paleozoic rocks in the subsurface of Nebraska.

Carlson, M. P. (1999). Transcontinental Arch—A pattern formed by rejuvenation of local features across central North America. *Tectonophysics*, *305*(1-3), 225-233. https://doi.org/10.1016/S0040-1951(99)00005-0

Clay, J. M., Moecher, D. P., & Bowersox, J. R. (2021). Detrital zircon U-Pb geochronology of the Precambrian Middle Run Formation (eastern North America basement): implications for Grenvillian foreland basin evolution and midcontinent rifting. *Precambrian Research*, *364*, 106332. https://doi.org/10.1016/j.precamres.2021.106332

Condon, D., Zhu, M., Bowring, S., Wang, W., Yang, A., & Jin, Y. (2005). U-Pb ages from the neoproterozoic Doushantuo Formation, China. *Science*, *308*(5718), 95-98. DOI: 10.1126/science.1107765

Cothren, H. R., Farrell, T. P., Sundberg, F. A., Dehler, C. M., & Schmitz, M. D. (2022). Novel age constraints for the onset of the Steptoean Positive Isotopic Carbon Excursion (SPICE) and the late Cambrian time scale using high-precision U-Pb detrital zircon ages. *Geology*, *50* (12), 1415-1420. https://doi.org/10.1130/G50434.1

Cox, G. M., Isakson, V., Hoffman, P. F., Gernon, T. M., Schmitz, M. D., Shahin, S., ... & Nordsvan, A. (2018). South Australian U-Pb zircon (CA-ID-TIMS) age supports globally synchronous Sturtian deglaciation. *Precambrian Research*, *315*, 257-263. https://doi.org/10.1016/j.precamres.2018.07.007

Fritz, W. H. (1968). Lower and early Middle Cambrian trilobites from the Pioche Shale, east-central Nevada. *USA Palaeontology*, *11*(2), 183-235.

Gans, P. B., & Miller, E. L. (1983). Style of mid-Tertiary extension in east-central Nevada: Utah Geology and Mineral Survey Special Studies, v. 59.

Gans, P. B., Miller, E. L., McCarthy, J., & Ouldcott, M. L. (1985). Tertiary extensional faulting and evolving ductile-brittle transition zones in the northern Snake Range and vicinity: New insights from seismic data. *Geology*, *13*(3), 189-193.

Gradstein, F. M., Ogg, J. G., Schmitz, M. D., & Ogg, G. M. (Eds.). (2020). *Geologic time scale 2020*. Elsevier.

Hodgin, E. B., Swanson-Hysell, N. L., DeGraff, J. M., Kylander-Clark, A. R., Schmitz, M. D., Turner, A. C., ... & Stolper, D. A. (2022). Final inversion of the Midcontinent Rift during the Rigolet Phase of the Grenvillian Orogeny. *Geology*, *50*(5), 547-551.

Horstwood, M.S., Košler, J., Gehrels, G., Jackson, S.E., McLean, N.M., Paton, C., Pearson, N.J., Sircombe, K., Sylvester, P., Vermeesch, P. and Bowring, J.F., 2016, Community-derived standards for LA-ICP-MS U-(Th-) Pb geochronology–Uncertainty propagation, age interpretation and data reporting: Geostandards and Geoanalytical Research, 40(3), p. 311-332.

Hose, R. K., & Blake, M. C. (1976). Geology of White Pine County, Nevada. *Nevada Bureau of Mines and Geology Bulletin*, *85*, 1-35.

Isakson, V. H., Schmitz, M. D., Dehler, C. M., Macdonald, F. A., & Adolph Yonkee, W. (2022). A robust age model for the Cryogenian Pocatello Formation of southeastern Idaho (northwestern USA) from tandem in situ and isotope dilution U-Pb dating of volcanic tuffs and epiclastic detrital zircons. *Geosphere*, *18*(2), 825-849. https://doi.org/10.1130/GES02437.1

Jackson, S.E., Pearson, N.J., Griffin, W.L. and Belousova, E.A., 2004, The application of laser ablation-inductively coupled plasma-mass spectrometry to in situ U–Pb zircon geochronology: Chemical geology, 211(1-2), p. 47-69.

Jones III, J. V., & Thrane, K. (2012). Correlating Proterozoic synorogenic metasedimentary successions in southwestern Laurentia: New insights from detrital zircon U-Pb geochronology of Paleoproterozoic quartzite and metaconglomerate in central and northern Colorado, USA. *Rocky Mountain Geology*, *47*(1), 1-35. https://doi.org/10.2113/gsrocky.47.1.1

Karlstrom, K. E., Mohr, M. T., Schmitz, M. D., Sundberg, F. A., Rowland, S. M., Blakey, R., ... & Hagadorn, J. W. (2020). Redefining the Tonto Group of Grand Canyon and recalibrating the Cambrian time scale. *Geology*, *48*(5), 425-430. https://doi.org/10.1130/G46755.1

Keeley, J. A., Link, P. K., Fanning, C. M., & Schmitz, M. D. (2013). Pre-to synglacial rift-related volcanism in the Neoproterozoic (Cryogenian) Pocatello Formation, SE Idaho: New SHRIMP and CA-ID-TIMS constraints. *Lithosphere*, *5*(1), 128-150. https://doi.org/10.1130/L226.1

Kylander-Clark, A.R., Hacker, B.R. and Cottle, J.M., 2013, Laser-ablation split-stream ICP petrochronology: Chemical Geology, 345, p. 99-112.

Long, S. P., Lee, J., & Blackford, N. R. (2022). The low-angle breakaway system for the Northern Snake Range décollement in the Schell Creek and Duck Creek Ranges, eastern Nevada, USA: Implications for displacement magnitude. *Geosphere*, *18*(4), 1194-1222.

Macdonald, F. A., Schmitz, M. D., Crowley, J. L., Roots, C. F., Jones, D. S., Maloof, A. C., ... & Schrag, D. P. (2010). Calibrating the cryogenian. *science*, *327*(5970), 1241-1243.

Macdonald, F. A., Yonkee, W. A., Flowers, R. M., & Swanson-Hysell, N. L. (2022). Neoproterozoic of laurentia. In *Laurentia: Turning Points in the Evolution of a Continent*. Geological Society of America. https://doi.org/10.1130/2022.1220(19)

MacLennan, S., Park, Y., Swanson-Hysell, N., Maloof, A., Schoene, B., Gebreslassie, M., ... & Haileab, B. (2018). The arc of the Snowball: U-Pb dates constrain the Islay anomaly and the initiation of the Sturtian glaciation. *Geology*, *46*(6), 539-542. https://doi.org/10.1130/G40171.1

Mahatma, A. A., Kuiper, Y. D., & Holm-Denoma, C. S. (2022). Evidence for the~ 1.4 Ga Picuris orogeny in the central Colorado Front Range. *Precambrian Research*, *382*, 106878. https://doi.org/10.1016/j.precamres.2022.106878

Mahon, R. C., Dehler, C. M., Link, P. K., Karlstrom, K. E., & Gehrels, G. E. (2014). Geochronologic and stratigraphic constraints on the Mesoproterozoic and Neoproterozoic Pahrump Group, Death Valley, California: A record of the assembly, stability, and breakup of Rodinia. *Bulletin*, *126*(5-6), 652-664.

Medaris Jr, L. G., Singer, B. S., Jicha, B. R., Malone, D. H., Schwartz, J. J., Stewart, E. K., ... & Reiners, P. W. (2021). Early Mesoproterozoic evolution of midcontinental Laurentia: Defining the geon 14 Baraboo orogeny. *Geoscience Frontiers*, *12*(5), 101174. https://doi.org/10.1016/j.gsf.2021.101174

Miller, D. M., & Lush, A. P. (1994). *Geologic map of the pilot peak quadrangle, box Elder County, Utah, and Elko County, Nevada*. The Survey.

Misch, P., & Hazzard, J. C. (1962). Stratigraphy and metamorphism of late Precambrian rocks in central northeastern Nevada and adjacent Utah. *AAPG Bulletin*, *46*(3), 289-343. https://doi.org/10.1306/BC743823-16BE-11D7-8645000102C1865D

Nelson, L. L., Smith, E. F., Hodgin, E. B., Crowley, J. L., Schmitz, M. D., & Macdonald, F. A. (2020). Geochronological constraints on Neoproterozoic rifting and onset of the Marinoan glaciation from the Kingston Peak Formation in Death Valley, California (USA). *Geology*, *48*(11), 1083-1087. https://doi.org/10.1130/G47668.1

Paton, C., Woodhead, J.D., Hellstrom, J.C., Hergt, J.M., Greig, A. and Maas, R., 2010, Improved laser ablation U-Pb zircon geochronology through robust downhole fractionation correction: Geochemistry, Geophysics, Geosystems, *11*(3).

Peak, B. A., Flowers, R. M., & Macdonald, F. A. (2023). Ediacaran-Ordovician tectonic and geodynamic drivers of Great Unconformity exhumation on the southern Canadian Shield. *Earth and Planetary Science Letters*, *619*, 118334. https://doi.org/10.1016/j.epsl.2023.118334

Poole, F. G., Perry, W. J., Madrid, R. J., & Amaya-Martínez, R. (2005). Tectonic synthesis of the Ouachita-Marathon-Sonora orogenic margin of southern Laurentia: Stratigraphic and structural implications for timing of deformational events and plate-tectonic model. https://doi.org/10.1130/0-8137-2393-0.543

Prave, A. R., Condon, D. J., Hoffmann, K. H., Tapster, S., & Fallick, A. E. (2016). Duration and nature of the end-Cryogenian (Marinoan) glaciation. *Geology*, *44*(8), 631-634. https://doi.org/10.1130/G38089.1

Pu, J. P., Bowring, S. A., Ramezani, J., Myrow, P., Raub, T. D., Landing, E., ... & Macdonald, F. A. (2016). Dodging snowballs: Geochronology of the Gaskiers glaciation and the first appearance of the Ediacaran biota. *Geology*, *44*(11), 955-958. https://doi.org/10.1130/G38284.1

Rainbird, R., Cawood, P., & Gehrels, G. (2011). The great Grenvillian sedimentation episode: record of supercontinent Rodinia's assembly. *Tectonics of sedimentary basins: Recent advances*, 583-601. https://doi.org/10.1002/9781444347166.ch29

Rodgers, D. W. (1984). Stratigraphy, correlation, and depositional environments of Upper Proterozoic and Lower Cambrian rocks of the southern Deep Creek Range, Utah.

Rooney, A. D., Macdonald, F. A., Strauss, J. V., Dudás, F. Ö., Hallmann, C., & Selby, D. (2014). Re-Os geochronology and coupled Os-Sr isotope constraints on the Sturtian snowball Earth. *Proceedings of the National Academy of Sciences*, *111*(1), 51-56. https://doi.org/10.1073/pnas.1317266110

Rooney, A. D., Cantine, M. D., Bergmann, K. D., Gómez-Pérez, I., Al Baloushi, B., Boag, T. H., ... & Strauss, J. V. (2020). Calibrating the coevolution of Ediacaran life and environment. *Proceedings of the National Academy of Sciences*, *117*(29), 16824-16830. https://doi.org/10.1073/pnas.2002918117

Rooney, A. D., Yang, C., Condon, D. J., Zhu, M., & Macdonald, F. A. (2020). U-Pb and Re-Os geochronology tracks stratigraphic condensation in the Sturtian snowball Earth aftermath. *Geology*, *48*(6), 625-629. https://doi.org/10.1130/G47246.1

Schneck, W. M. (1986). *Lithostratigraphy of the McCoy Creek Group and Prospect Mountain Quartzite (upper Proterozoic and Lower Cambrian), Egan and Cherry Creek Ranges, White Pine County, Nevada* (Doctoral dissertation, Eastern Washington University).

Schoene, B., Eddy, M.P., Samperton, K.M., Keller, C.B., Keller, G., Adatte, T. and Khadri, S.F., 2019, U-Pb constraints on pulsed eruption of the Deccan Traps across the end-Cretaceous mass extinction: Science, 363(6429), p. 862-866. doi:10.1126/science.aau2422

Sloss, L. L. (1988). Tectonic evolution of the craton in Phanerozoic time. *The Geology of North America*, *2*, 25-51.

Southwick, D. L., Morey, G. B., & Mossler, J. H. (1986). Fluvial origin of the lower Proterozoic Sioux Quartzite, southwestern Minnesota. *Geological Society of America Bulletin*, *97*(12), 1432-1441. https://doi.org/10.1130/0016-7606(1986)97<1432:FOOTLP>2.0.CO;2

Spencer, C. J., Prave, A. R., Cawood, P. A., & Roberts, N. M. (2014). Detrital zircon geochronology of the Grenville/Llano foreland and basal Sauk Sequence in west Texas, USA. *Bulletin*, *126*(7-8), 1117-1128.

Timmons, J. M., Bloch, J., Fletcher, K., Karlstrom, K. E., Heizler, M., & Crossey, L. J. (2012). The Grand Canyon Unkar Group: Mesoproterozoic basin formation in the continental interior during supercontinent assembly. *Grand Canyon Geology*, *2*, 25-48.

Vermeesch, P., 2018, IsoplotR: A free and open toolbox for geochronology: Geoscience Frontiers, 9(5), p. 1479-1493.

Vermeesch, P. (2020). On the treatment of discordant detrital zircon U–Pb data. *Geochronology Discussions*, *2020*, 1-19. https://doi.org/10.5194/gchron-3-247-2021

Wiedenbeck, M.A.P.C., Alle, P., Corfu, F.Y., Griffin, W.L., Meier, M., Oberli, F.V., Quadt, A.V., Roddick, J.C. and Spiegel, W., 1995, Three natural zircon standards for U-Th-Pb, Lu-Hf, trace element and REE analyses: Geostandards newsletter, 19(1), p. 1-23.

Wendt, I. and Carl, C., 1991, The statistical distribution of the mean squared weighted deviation: Chemical Geology: Isotope Geoscience Section, 86(4), p. 275-285.

Woodward, L. A. (1963). Late Precambrian metasedimentary rocks of Egan range, Nevada. *AAPG Bulletin*, *47*(5), 814-822.

Woodward, L. A. (1965). Late Precambrian stratigraphy of northern Deep Creek Range, Utah. *AAPG Bulletin*, *49*(3), 310-316.

Woodward, L. A. (1967). Stratigraphy and correlation of late Precambrian rocks of Pilot Range, Elko County, Nevada, and Box Elder County, Utah. *AAPG Bulletin*, *51*(2), 235-243.

Yonkee, W. A., Dehler, C. D., Link, P. K., Balgord, E. A., Keeley, J. A., Hayes, D. S., ... & Johnston, S. M. (2014). Tectono-stratigraphic framework of Neoproterozoic to Cambrian strata, west-central US: Protracted rifting, glaciation, and evolution of the North American Cordilleran margin. *Earth-Science Reviews*, *136*, 59-95. https://doi.org/10.1016/j.earscirev.2014.05.004

Young, J. C. (1960). Structure and stratigraphy in north central Schell Creek Range.

Zhang, T., Keller, C. B., Hoggard, M. J., Rooney, A. D., Halverson, G. P., Bergmann, K. D., ... & Strauss, J. V. (2023a). A Bayesian framework for subsidence modeling in sedimentary basins: A case study of the Tonian Akademikerbreen Group of Svalbard, Norway. *Earth and Planetary Science Letters*, *620*, 118317. https://doi.org/10.1016/j.epsl.2023.118317

Zhang, T., Keller, C.B., Strauss, J.V. (2023b), SubsidenceChron.jl. https://doi.org/10.17605/OSF.IO/ZW5GA